Representing Subgrid Snow Cover Heterogeneities in Regional and Global Models

GLEN E. LISTON

Department of Atmospheric Science, Colorado State University, Fort Collins, Colorado

(Manuscript received 5 May 2003, in final form 30 September 2003)

ABSTRACT

To improve the depiction of autumn through spring land–atmosphere interactions and feedbacks within regional and global weather, climate, and hydrologic models, a Subgrid SNOW Distribution (SSNOWD) submodel that explicitly includes subgrid snow-depth and snow-cover variability has been developed. From both atmospheric and hydrologic perspectives, the subgrid snow-depth distribution is an important quantity to account for within large-scale models. In the natural system, these subgrid snow-depth distributions are largely responsible for the mosaic of snow-covered and snow-free areas that develop as the snow melts, and the impacts of these fractional areas must be quantified in order to realistically simulate grid-averaged surface fluxes. SSNOWD's formulation incorporates observational studies showing that snow distributions can be described by a lognormal distribution and the snow-depth coefficient of variation. Using an understanding of the physical processes that lead to these observed snow-depth variations, a global distribution of nine subgrid snow-depth-variability categories was developed, and coefficient-of-variation values were assigned to each category based on published measurements. In addition, SSNOWD adopts the physically realistic approach of performing separate surface-energy-balance calculations over the snow-covered and snow-free portions of each model grid cell and weighing the resulting fluxes according to these fractional areas. Using a climate version of the Regional Atmospheric Modeling System (ClimRAMS) over a North American domain, SSNOWD was compared with a snow-cover formulation similar to those currently used in most general circulation models. The simulations indicated that accounting for snow-distribution variability has a significant impact on snow-cover evolution and associated energy and moisture fluxes.

1. Introduction

Snow distributions in mid- and high-latitude landscapes play a key role in defining energy and moisture relationships associated with earth's climate system. Numerous observational and modeling studies have demonstrated the importance of snow on a number of atmospheric and land surface features and processes, such as air temperature, precipitation, soil temperature and moisture, and vegetation. These studies have ranged from *local* (e.g., Wagner 1973; Baker et al. 1992), to *regional* (e.g., Dewey 1977; Ellis and Leathers 1999), to *subcontinental* (e.g., Namias 1985; Walsh et al. 1985), and to *continental* and *global* (e.g., Karl et al. 1993; Bamzai and Shukla 1999). In light of the role that snow plays in influencing land and atmospheric processes, it is essential that local, regional, and global models used to simulate weather, climate, and hydrologic interactions be capable of accurately describing seasonal snow evolution.

Recently, significant strides have been made toward developing more complex and physically realistic snow models for use within large-scale atmospheric models (e.g., Verseghy 1991; Lynch-Stieglitz 1994; Marshall and Oglesby 1994; Marshall et al. 1994; Douville et al. 1995; Yang et al. 1997; Loth and Graf 1998a; Slater et al. 1998; Essery et al. 1999b; Jin et al. 1999; Sun et al. 1999; Roesch et al. 2001; Takata et al. 2003), but current models still suffer from significant misrepresentations of snow-related features, distributions, and processes (e.g., Foster et al. 1996; Frei and Robinson 1998; Slater et al. 1998; Roesch et al. 1999; Pitman 2003). Typically, snow accumulation and snowmelt in climate models are simulated by applying simple energy- and mass-balance accounting procedures (Foster et al. 1996), and most recent model improvements have focused on adding vertical resolution and improved one-dimensional (vertical) physics. These algorithms frequently neglect or oversimplify important physical processes, such as those associated with subgrid-scale temporal and spatial variability of the snow-covered area. The lack of subgrid snow-distribution representations in most climate models has been identified as a deficiency in snow-cover evolution and atmospheric interaction simulations (Loth and Graf 1998b; Pomeroy et al. 1998; Slater et al. 2001; Takata et al. 2003).

Corresponding author address: Dr. Glen E. Liston, Department of Atmospheric Science, Colorado State University, Fort Collins, CO 80523-1371.
E-mail: liston@atmos.colostate.edu

2. Background

a. Subgrid snow distribution mechanisms

Snow depths around the world vary greatly at subgrid scales [i.e., scales smaller than the typical horizontal grid increment of regional (5–50) or global (50–500 km) atmospheric models; e.g., McKay and Gray (1981)]. During the snow accumulation season, spatial snow-depth variations over land are primarily the result of three mechanisms: 1) snow–canopy interactions in forested regions, 2) snow redistribution by wind, and 3) orographic influences on solid precipitation. These three factors operate at distinctly different spatial scales.

In relatively flat, forested landscapes, snow distribution mechanisms operate at scales of one to hundreds of meters. In this environment, canopy-intercepted snow can lose mass by sublimation and snow released from branches accumulates on the ground in nonuniform snow-depth patterns (Sturm 1992; Hedstrom and Pomeroy 1998; Pomeroy et al. 2002). These accumulation variations depend on leaf area, species composition, and canopy density differences, all of which span the full range of variability from dense evergreen canopies to treeless clearings.

At distances of tens to hundreds of meters, wind-blown snow is a dominant factor influencing the snow distribution in tundra, prairie, and alpine/mountain snow covers (e.g., Sturm et al. 1995). In these environments, the frequent occurrence of blowing snow leads to significant snow redistribution, causing it to accumulate in the lee of ridges, topographic depressions, and taller vegetation (e.g., Elder et al. 1991; Pomeroy et al. 1993; Liston and Sturm 1998; Sturm et al. 2001a,b; Liston et al. 2002; Hiemstra et al. 2002). A further consequence of these blowing-snow events is that significant portions (10%–50%) of the snow cover are returned to the atmosphere by sublimation of the wind-borne snow particles (Liston and Sturm 1998, 2002; Essery et al. 1999a; Pomeroy and Essery 1999).

At a larger scale, orographic precipitation influences snow depths over distances of one to a few kilometers (e.g., Barros and Lettenmaier 1994; Leung and Ghan 1995). The nonuniform snow distributions produced by orographic precipitation are due to differences in local wind fields, atmospheric stability, and moisture distributions resulting from interactions with the topography. These factors, in turn, influence cloud microphysical processes associated with precipitation. Frequently, snowfall events are associated with the presence of synoptic-scale atmospheric disturbances like cyclones and their associated frontal boundaries. The mountains reduce the storm's movement and lead to rising air as it moves over the topographic barrier. Orography also modifies snow distributions through temperature influences on the snow line.

During snowmelt, spatially variable melt processes further modify the snow distribution. One of the most significant of these is the difference in available solar radiation resulting from slope and aspect relationships; in the Northern Hemisphere, for example, south-facing slopes receive more solar radiation and thus snow generally melts faster there than snow on north-facing slopes. Vegetation and surrounding topography also play a role in producing heterogeneous melt patterns, by shading snow and by emitting longwave radiation (Olyphant 1986). Local advection can also produce enhanced snowmelt (e.g., Olyphant and Isard 1988). This influence can be greatest at the leading edges of snow patches, thus leading to further snow-depth variations (Liston 1995).

In addition to the main factors described above, other natural and human-related factors influence snow distributions. These include snow avalanches (Elder et al. 1991) and the plowing of roads and parking lots. For economic reasons, people have also developed ways to enhance snow accumulations to benefit agriculture. These include modifying winter vegetation cover and building hedges and snow fences to capture wind-transported snow (Pomeroy and Gray 1995).

b. Impact of nonuniform snow covers

The nonuniform snow covers that dominate earth's natural system have important influences on atmospheric and hydrologic processes. The thermal conductivity of snow is substantially lower than other naturally occurring substances like soil, rock, ice, and liquid water. Thus, the presence of snow generally reduces conductive energy exchanges between the atmosphere and ground (Zhang et al. 1996; Taras et al. 2002), ice-covered inland water (Jeffries et al. 1999), and ice-covered oceans (Sturm et al. 2002b).

During the melt of a nonuniform snow cover, snow-depth variations lead to a mosaic of snow-free and snow-covered areas that evolve as the snow melts. When an area is not completely snow covered, the contrast between the snow-covered area and snow-free surface (e.g., vegetation, rock, or soil) strongly affects the local surface energy balance (Liston 1995, 1999; Essery 1997). This influence is due to three primary differences between the energy balances of snow-covered and snow-free surfaces. For the snow-covered case 1) a melting surface cannot rise above the freezing temperature; associated with this is 2) a nonzero melt term. In addition, 3) the snow albedo is generally much larger than the snow-free albedo. Secondary differences are related to other properties of the two surfaces, such as roughness-length differences and the insulating character of the snow cover. Thus, snow-covered area variations can strongly modify energy and moisture flux interactions between land and atmosphere.

To highlight the importance of snow-covered versus snow-free regions in a model grid cell, fluxes over snow-covered and snow-free areas were calculated using the Liston et al. (1999) surface-energy-balance model and the following forcing conditions: air temperature $= -3^{\circ}$

and +3°C, for nonmelting and melting cases, respectively; albedo = 0.8, 0.6, and 0.15, for nonmelting snow, melting snow, and snow-free cases, respectively; midday solar radiation conditions at 47°N latitude; and general values of relative humidity, wind speed, cloud-cover fraction, and roughness length. For nonmelting conditions, when the grid cell was greater than 15% snow free, the latent heat flux from the snow-free surface dominated that over the snow surface during the autumn, winter, and spring. The sensible heat flux over that snow-free surface was greater than the snow-covered fraction during autumn and spring when the grid cell was between 0% and 10% snow free. During winter, when incoming solar radiation was minimal, the sensible heat flux changed sign from the autumn and spring cases and was toward the snow surface and away from the snow-free surface. Under melting conditions, when just a small fraction of the grid cell (a few percent) was snow free, the latent heat flux over that snow-free area surpassed the flux associated with the snow-covered fraction. The sensible heat flux under melting conditions was generally toward the snow-covered surface, and the snow-free fraction had the opposite sign. Therefore, knowledge of the snow-covered and snow-free surface fractions is crucial to correctly define the magnitude and direction of grid-averaged surface fluxes under both melting and nonmelting conditions.

As a further example of the need to account for subgrid snow distributions, Liston (1999) compared a typical atmospheric model snow-distribution representation with a corresponding observed snow distribution. The typical model representation had errors of ± 60 W m^{-2} in net solar radiation, ± 10 W m^{-2} in net longwave radiation, ± 80 W m^{-2} in sensible plus latent energy flux, and ± 40 W m^{-2} in melt energy.

In light of the important roles that nonuniform snow distributions play within climate and hydrologic systems, methods must be developed to simulate the relevant features, processes, and interactions. This paper presents a snow model that accounts for subgrid snow distributions within large-scale atmospheric and hydrologic models. The subgrid snow model is tested within a regional atmospheric model, and model strengths and limitations are discussed.

3. Subgrid SNOW Distribution (SSNOWD) model

Primary considerations for developing this model included 1) representing the first-order effects of nonuniform snow distributions, 2) easy implementation within virtually any regional to global atmospheric or hydrologic model, and 3) computational efficiency. With its focus on subgrid-scale snow distributions, the model is called the Subgrid SNOW Distribution (SSNOWD; pronounced ''snow-dee'') model or parameterization. To simplify the following discussion it is assumed that the bulk, or vertically integrated, average snow density is known; thus, the terms ''snow depth'' or ''snow-water-equivalent depth'' will be used interchangeably, with the understanding that the snow depths can be converted to a snow-water-equivalent depth by multiplying by the snow and water density ratio.

a. Model requirements and assumptions

At its most basic foundation, SSNOWD must fulfill three basic requirements: 1) produce grid-scale surface energy and moisture fluxes, 2) account for snow accumulation, and 3) account for snowmelt. Inherent in this formulation is the fact that the subgrid snow-distribution model must be driven with grid-averaged (or grid scale) atmospheric forcing fields (e.g., snow precipitation and melt rates), and it must output grid-averaged (or grid scale) surface fluxes for use by the host atmospheric or hydrologic model.

1) REQUIREMENT 1: *PRODUCE APPROPRIATE GRID-SCALE ENERGY AND MOISTURE FLUXES AT THE TERRESTRIAL–ATMOSPHERE INTERFACE*

In a study examining the complex interactions among snow-covered areas, snow-free areas, and the atmosphere, Liston (1995) found increasingly nonlinear snowmelt rates as snow-covered area decreased. While the remaining snow melted faster as the snow-free area increased, its impact on the atmosphere became less significant with decreasing snow-covered area. From the perspective of the atmosphere (or the grid-averaged melt rate), the behavior was essentially linear (within a few percent; see Fig. 10 of Liston 1995). Therefore, to satisfy requirement 1, SSNOWD assumes linear behavior and calculates one energy balance assuming the grid cell is snow covered, calculates a second balance assuming the grid cell is snow free (assuming both calculations see the same atmosphere) and linearly weights the resulting surface fluxes in proportion to the snow-covered (Γ) and snow-free fractions, that is,

$$Q_{ga} = \Gamma Q_{sc} + (1 - \Gamma) Q_{sf}, \tag{1}$$

where, for any flux variable Q, Q_{ga} is the grid-averaged flux, Q_{sc} is the snow-covered flux, and Q_{sf} is the snow-free flux.

In contrast to this approach, most large-scale atmospheric models define snow-covered and snow-free grid-cell fractions that are only used to linearly weight the albedo and then apply this albedo to a single snow-covered energy balance computation per grid cell (the fluxes are not fractionally weighted according to snow-covered and snow-free fractions). This procedure is physically inappropriate because the energy balances over snow-covered and snow-free areas are not identical. Using the atmospheric conditions and model described in section 2b, but for melting conditions on 1 May only, the errors imposed by using such a procedure, compared with the fractional snow-cover weighting approach used by SSNOWD, are highlighted in Fig. 1.

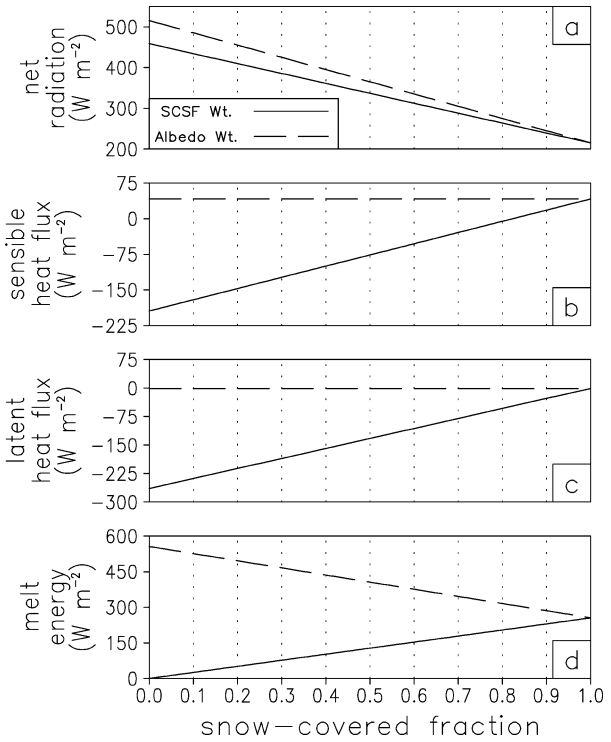

FIG. 1. Comparison of (a) net radiation, (b) sensible heat flux, (c) latent heat flux, and (d) melt energy, resulting from 1) calculating separate energy balances over the snow-covered and snow-free portions of the grid cell and weighting the resulting fluxes according to the snow-covered and snow-free fractions (SCSF wt.), and 2) assuming that the snow-covered and snow-free grid-cell fractions are only used to linearly weigh the albedo and then applying this albedo to a single snow-covered energy-balance computation (albedo wt.). Fluxes toward the surface are defined to be positive. The difference between the two net radiation curves is the difference between the outgoing longwave radiation for the two cases. The distance between the two curves in (a)–(d) gives the increase in error, with decreasing snow-covered fraction, imposed by taking the albedo wt. approach.

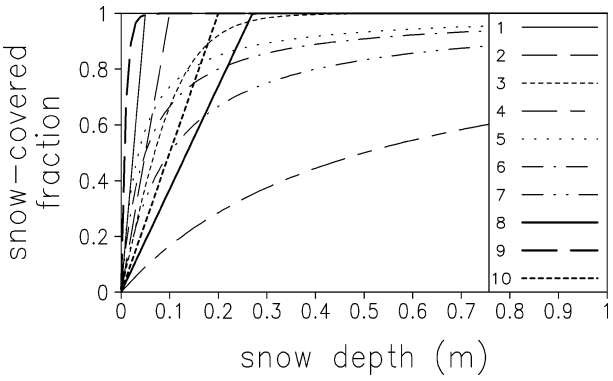

FIG. 2. Example snow-covered fraction parameterizations used within 14 land surface submodels and large-scale atmospheric models. Profiles were computed for conditions of a 0.05-m roughness length (short vegetation) and a 280 kg m^{-3} snow density (Liston and Pielke 2001). Listed are the associated land surface and atmospheric model names and references. 1) LSM/CCM3 (Bonan 1996), ECHAM (Loth and Graf 1998a); 2) CLASS/CCC (Verseghy 1991), ClimRAMS (Liston and Pielke 2001); 3) BATS (Yang et al. 1997); 4) BATS/CCM2,3 (Dickinson et al. 1993), CLM/CCM3 (Zeng et al. 2002; Dai et al. 2003); 5) ARPEGE (Douville et al. 1995), ECHAM4 (Roesch et al. 1999); 6) CCM1 (Marshall and Oglesby 1994); 7) CCM0A (Marshall et al. 1994); 8) SIB2/CSU (Sellers et al. 1996); 9) EM (Edelmann et al. 1995); 10) BASE (Slater et al. 1998).

The errors in net radiation, sensible and latent heat fluxes, and melt energy increase linearly with decreasing snow-covered fraction. As one would expect, decreasing the snow albedo leads to very high melt-energy values, and this melt energy is available through reduced outgoing longwave radiation and sensible and latent heat flux quantities. This traditional approach significantly misrepresents surface energy exchanges in the natural system.

2) REQUIREMENT 2: *ACCOUNT FOR SNOW ACCUMULATION PROCESSES*

For a given location, from year to year, the factors that influence the snow accumulation and distribution *patterns* are generally the same (Kirnbauer and Blöschl 1994; Sturm et al. 1995). These factors are typically climate related and include chronic trends in wind speed and direction, precipitation–topography relationships, and air temperatures. These relatively similar forcing conditions lead to snow patterns that are location specific and show little interannual variation at each location, while the snow *depths* can vary from one year to the next. For example, in the Rocky Mountains of the United States, winter storm winds typically have a strong westerly component. This westerly flow leads to greatest orographic precipitation accumulation on the west-facing slopes, and alpine blowing–snow accumulation on east-facing slopes. While snow depths in the Rocky Mountains can vary significantly from year to year, the time-invariant topography, along with the westerly jet stream, produce similar yearly snow distribution patterns.

Since a reasonable first-order approximation is that snow-depth distribution patterns are time invariant, model requirement 2 can be satisfied by predefining the snow-depth distribution patterns, in a statistical sense, used by the model. These variations must be defined in a way that includes processes such as snow–canopy interactions, wind redistribution, and orographic influences on snow distributions. Because of the numerous factors (and the scales at which they operate) influencing snow-depth distributions in the natural system, these distribution patterns will vary widely over the globe.

In contrast, most current large-scale atmospheric models employ simplistic empirical functions to define snow-depth distributions. Figure 2 displays the parameterizations used in one regional atmospheric model and 13 land surface hydrology models and their associated general circulation models (GCMs). While some of these have simple roughness-length dependencies, these relationships typically do not vary from one region of

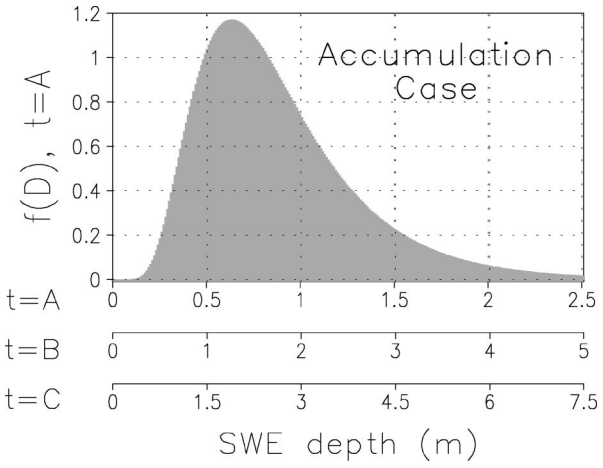

FIG. 3. Conceptual illustration of the SSNOWD assumption that solid precipitation (snowfall) reaching a surface grid cell has a prescribed spatial distribution that is represented by a snow-water-equivalent (SWE) depth probability distribution function, $f(D)$. The shape of this function has no temporal variation, and the total amount of snow represented by the function is given by the cell-average-accumulated snowfall input at time, t. This example has cell-mean SWE values of 0.9, 1.8, and 2.7 m, at t = A, B, and C, respectively. Only $f(D)$ values at t = A are shown on the vertical axis; because $f(D)$ is normalized, its values also vary with mean SWE.

the world to another. Clearly, from our discussion of the various factors that influence snow-depth distribution patterns over a wide range of scales, the curves in Fig. 2 cannot be (realistically) globally applicable. In an effort to correct this deficiency, Roesch et al. (2001) introduced a method to account for snow-distribution differences by considering three basic terrain types across the globe: flat nonforested areas, mountainous nonforested areas, and forests.

SSNOWD assumes that all solid precipitation (snowfall) reaching the surface accumulates following a subgrid snow distribution that is invariant with total accumulation value. All snowfall accumulating in each model grid cell has a prescribed spatial distribution that can be represented in the form of a probability distribution function (pdf) that has no temporal variation. The total amount of snow represented by that pdf is given by the grid-cell-average snowfall inputs. Figure 3 provides a conceptual illustration of this approach.

3) REQUIREMENT 3: *ACCOUNT FOR SNOW ABLATION (MELT) PROCESSES*

As indicated previously, spatially variable melt processes, associated with differences in radiation reaching the snow surface, can generate snow-depth distribution variations. In spite of these spatially variable melt influences, the snow distribution itself is the dominant factor that determines the spatial patterns of snow-covered and snow-free areas during any melt period. In the simplest terms, the shallowest snow disappears first, while the deepest snow disappears last. In addition to being an initial condition that defines the snow distribution at the beginning of the melt period, the premelt snow distribution is a boundary condition that persists throughout the melt period until the snow cover ablates. Liston (1999) demonstrated that three fundamental features are required to describe the evolution of seasonal snow cover within a model grid cell: 1) the within-grid snow-water-equivalent distribution, 2) the grid-cell-averaged melt rate, and 3) the within-grid depletion of snow-covered area. In addition, Liston (1999) defined the mathematical interrelationships among these three features and demonstrated how to use any two features to generate the third. These interrelationships are employed in SSNOWD.

Typically, large-scale atmospheric and hydrologic models calculate a grid-cell-averaged snowmelt quantity, at each time step, for each grid cell (the snowmelt rate is assumed to be spatially constant across the entire grid cell). This approach is consistent with the fact that each grid cell in the models typically have only one air temperature, humidity, wind speed, etc., at any given point in time. Thus, SSNOWD assumes that the melt rate experienced over the snow-covered fraction, within each model grid cell, is spatially constant. Uniform melt over the grid cell means that the snow-covered area in that grid cell at the end of each model time step can be computed from the snow-distribution, snowmelt, and snow-cover depletion interrelationships outlined by Liston (1999). The ultimate effect of this assumption is that the example snow distribution (Fig. 3) shifts to the left in correspondence to accumulated melt depth (Fig. 4) and creates a snow-free fraction.

For relatively large grid cells in complex topographic regions it can be physically unrealistic to define a uniform melt rate over the entire grid cell (Luce and Tarboton 2001; Pomeroy et al. 2001, 2003). This assumption is typically made in atmospheric and hydrologic models and, for consistency, is adopted here. Factors, in addition to initial snow distribution, that affect snow-cover depletion all relate to variables that lead to spatial melt-rate variations. One way to mitigate the effect of this uniform melt-rate assumption is to decompose each model grid cell into subcell elevation bands where the melt rate is unique for each band (e.g., Hartman et al. 1999; Moore et al. 1999). In another approach, Walland and Simmonds (1996) used subgrid topographic information to determine the grid fraction that lies above the model freezing level for each grid cell, and they then divided the surface grid cells into melting and nonmelting fractions.

b. Model equations

Under the assumption of uniform melt depth, D_m, over a model grid cell, each cell includes a snow-free fraction and snow-covered fraction, $\Gamma(D_m)$, that sum to unity:

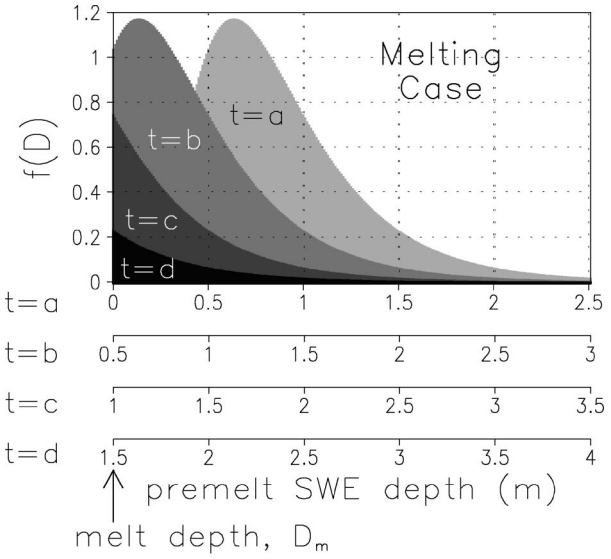

FIG. 4. Conceptual illustration of the SSNOWD assumption that the melt rate experienced over the snow-covered fraction, within each model grid cell, is spatially constant. This uniform melt leads to a snow distribution, $f(D)$, that shifts to the left by the accumulated melt depth, D_m, as indicated by the different times t = a, b, c, d. The snow-covered fraction is given by the area under the curves, in this case, 1.00, 0.84, 0.32, 0.09, for times a, b, c, and d, respectively.

$$\int_0^{D_m} f(D)\, dD + \int_{D_m}^{\infty} f(D)\, dD = 1. \tag{2}$$

Thus,

$$\Gamma(D_m) = 1 - \int_0^{D_m} f(D)\, dD, \tag{3}$$

where $f(D)$ is a snow-water-equivalent depth distribution function.

Numerous studies have found that observed snow depth and snow-water-equivalent depth distributions can be reasonably described by a two-parameter lognormal probability distribution function (e.g., Donald et al. 1995; Shook 1995; Pomeroy et al. 1998; Faria et al. 2000). Adopting this assumption, the distribution equation (Ang and Tang 1975) is given by (the following presentation corrects errors in Donald et al. 1995)

$$f(D) = \frac{1}{D\zeta\sqrt{2\pi}} \exp\left\{-\frac{1}{2}\left[\frac{\ln(D) - \lambda}{\zeta}\right]^2\right\} \tag{4}$$

with

$$\lambda = \ln(\mu) - \frac{1}{2}\zeta^2 \tag{5}$$

$$\zeta^2 = \ln(1 + \mathrm{CV}^2), \tag{6}$$

where D is snow-water-equivalent depth, and λ and ζ are distribution parameters related to the mean, μ, and coefficient of variation, CV (equal to the ratio of the standard deviation, σ, to the mean, μ), of the snow

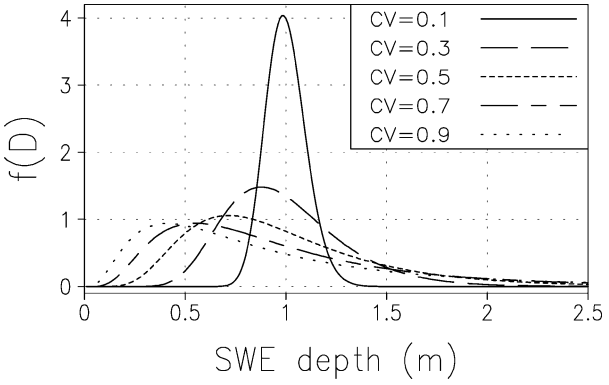

FIG. 5. The variation of the SWE depth function, $f(D)$, given by Eqs. (4)–(6), for different coefficient-of-variation, CV, values and a mean SWE depth of 1.0 m.

distribution under conditions of 100% grid-cell coverage (no melting has occurred). Figure 5 illustrates the variation of the function given by Eqs. (4)–(6).

Following Donald et al. (1995), combining Eqs. (3) and (4) yields the snow-covered area as a function of melt depth:

$$\Gamma(D_m) = 1 - \int_0^{D_m} \frac{1}{D\zeta\sqrt{2\pi}} \times \exp\left\{-\frac{1}{2}\left[\frac{\ln(D) - \lambda}{\zeta}\right]^2\right\} dD. \tag{7}$$

Changing the integration variable from D to z by the substitution

$$z = \frac{\ln(D) - \lambda}{\zeta} \tag{8}$$

yields

$$\Gamma(D_m) = 1 - \int_{-\infty}^{z_{D_m}} \frac{1}{\sqrt{2\pi}} e^{[-(1/2)z^2]}\, dz. \tag{9}$$

Expanding this produces

$$\Gamma(D_m) = 1 - \left\{\int_{-\infty}^{0} \frac{1}{\sqrt{2\pi}} e^{[-(1/2)z^2]}\, dz + \int_0^{z_{D_m}} \frac{1}{\sqrt{2\pi}} e^{[-(1/2)z^2]}\, dz\right\}, \tag{10}$$

where the first integral on the right-hand side corresponds to the left half of the cumulative distribution function of a Gaussian random variable; thus, because it has even symmetry, this first integral equals 0.5. Making a second substitution of $z = \sqrt{2}u$, and noting that the error function (erf) and the complementary error function (erfc; i.e., 1 − erf), are defined to be

$$\text{erf(CV)} = \frac{2}{\sqrt{\pi}} \int_0^{\text{CV}} e^{(-u^2)}\, du \tag{11}$$

$$\text{erfc(CV)} = \frac{2}{\sqrt{\pi}} \int_{\text{CV}}^{\infty} e^{(-u^2)}\, du \tag{12}$$

leads to

$$\Gamma(D_m) = \frac{1}{2}\,\text{erfc}\left(\frac{z_{D_m}}{\sqrt{2}}\right). \tag{13}$$

These error functions are commonly available as intrinsic functions in computational computer programming languages.

The average depth, D_a, over a grid cell experiencing a snowmelt depth, D_m, is given by (Donald et al. 1995)

$$D_a(D_m) = \int_0^{D_m} 0[f(D)]\, dD + \int_{D_m}^{\infty} (D - D_m)[f(D)]\, dD. \tag{14}$$

Expanding the second integral, and using Eqs. (2) and (3), yields

$$D_a(D_m) = \int_{D_m}^{\infty} D[f(D)]\, dD - D_m\Gamma(D_m), \tag{15}$$

where the remaining integral is solved by inserting Eq. (4)

$$\int_{D_m}^{\infty} D[f(D)]\, dD = \int_{D_m}^{\infty} \frac{1}{\zeta\sqrt{2\pi}} \exp\left\{-\frac{1}{2}\left[\frac{\ln(D) - \lambda}{\zeta}\right]^2\right\} dD \tag{16}$$

and by substituting Eq. (8) to get

$$\int_{D_m}^{\infty} D[f(D)]\, dD = \int_{D_m}^{\infty} \frac{1}{\sqrt{2\pi}} e^{\lambda} e^{\xi^2/2} e^{[-(z-\xi)^2/2]}\, dz. \tag{17}$$

Making a second substitution of $z - \xi = \sqrt{2}u$, and combining it with Eq. (15) gives

$$D_a(D_m) = \frac{1}{2} e^{(\lambda+\xi^2/2)}\,\text{erfc}\left(\frac{z_{D_m} - \xi}{\sqrt{2}}\right) - D_m\Gamma(D_m). \tag{18}$$

SSNOWD consists of solving Eqs. (1), (5), (6), (8), (13), and (18) under the varying input conditions supplied by the host atmospheric or hydrologic model. To drive SSNOWD, three pieces of information are required: 1) mean accumulated snow-water-equivalent on the ground in the absence of any melt, μ; 2) accumulated snow-water-equivalent melt depth, D_m; and 3) coefficient of variation, CV, for each model grid cell within the model simulation domain.

Within the context of distributed atmospheric and hydrologic models, μ and D_m can be evolved by introducing two additional two-dimensional arrays. These arrays sum the atmospheric model–simulated snow accumulation (e.g., the solid precipitation) and snowmelt rates (in snow-water-equivalent depth units) for each grid cell, at each model time step. In the event that the accumulated snowmelt depth leads to the complete removal of the snow cover, the arrays are reset to zero and the melt and depth accumulation accounting is reinitiated.

A special (but common) case occurs when new accumulation interrupts snowmelt. This situation can be addressed in two ways. The first option is to assume that the new snow falls over the entire grid cell, and that cell has an average snow depth equal to the new snow plus the cell-average snow depth from the fractional snow cover at the previous time step. However, this is physically unrealistic because it does not allow small snow accumulations to occur, melt, and reexpose the underlying surface in the middle of the melt period. Moore et al. (1999) presents a possible solution to this deficiency. The second option involves using the new accumulation to decrease melt-depth values, effectively pushing the depletion curve back toward 100% snow cover. Any additional snow accumulation after the melt depth, D_m, has been reduced to zero is added to the snow-depth value. This second option represents the ablation period more realistically but does not account for our assumption that snow precipitation is distributed over the entire grid cell. SSNOWD follows the second option. For melt periods that have occasional snow accumulations, option 2 generally produces smaller snow-covered fractions than option 1. A disadvantage with option 2 is that it lacks an analytical solution. When this occurs, SSNOWD uses a fast-converging fixed-point iteration algorithm to solve Eq. (18) for D_m when D_a is known.

Figure 6 displays the modeled variations in snow-covered fraction [Γ from Eq. (13)] and cell-average snow-water-equivalent depth [D_a from Eq. (18)] during melt, for $\mu = 1.0$ m and various CV values. As an example of implementing SSNOWD over an area (or a single model grid cell), Fig. 7 displays the precipitation and melt rate forcing, along with the associated accumulation (or summing) arrays. Figure 7 also shows the snow-covered fraction evolution when these forcings are applied to CV values of 0.1, 0.5, and 0.9. The smallest CV value maintained a continuous snow cover, while the melt event in December produced snow-covered fractions of 0.3–0.4 for the two largest CV values. During the April–May snow-cover depletion, the smallest CV value produced a snow-covered to snow-free transition that occurred over just a few days. In contrast, the two largest CV values took nearly two months to ablate the snow cover.

c. Model parameter distribution and values

The third piece of information required to run SSNOWD is knowledge of the CV distribution over the

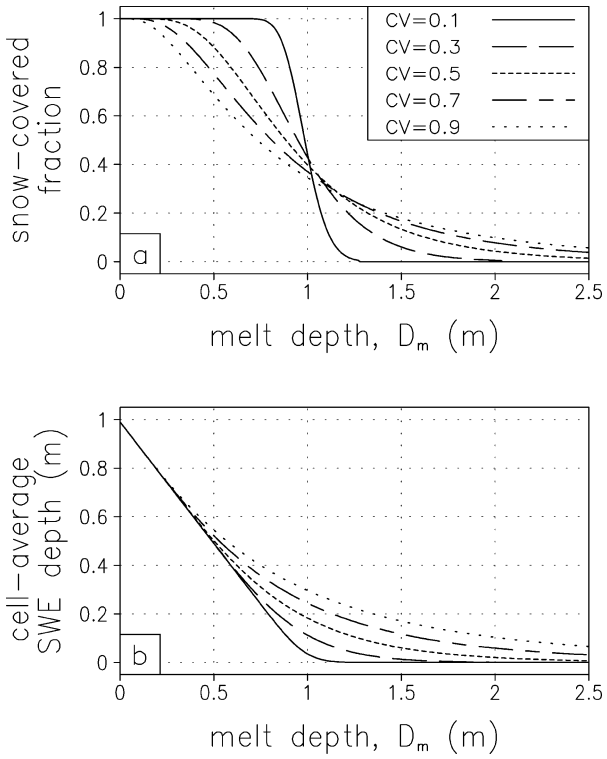

FIG. 6. SSNOWD variation in (a) snow-covered fraction and (b) cell-average SWE depth during melt, for a premelt mean SWE depth = 1.0 m and various coefficient-of-variation, CV, values.

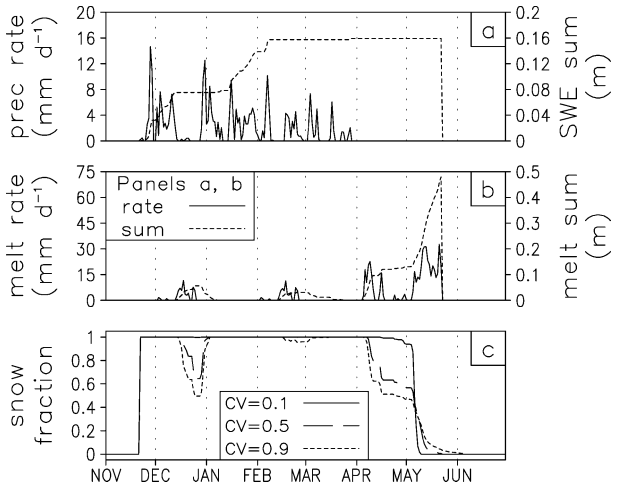

FIG. 7. Example SSNOWD simulation for a single model grid cell. Showing (a) the SWE precipitation and the sum of those values, (b) the SWE melt rates and the sum of those values, and (c) the evolution of snow-covered fraction when these forcings are applied to coefficient-of-variation, CV, values of 0.1, 0.5, and 0.9. In Feb and Mar, the SWE sum curve does not increase in response to the precipitation because it is balanced by melt during the same period.

atmospheric or hydrologic model domain. We define this distribution by recognizing three main factors that influence snow-depth variability: first, air temperature directly influences solid precipitation amounts; second, topographic variability affects solid orographic precipitation patterns; and third, wind speed influences snow redistribution by wind. To generate a global snow-depth variability map using these three influences, a dichotomous key was implemented to define nine different snow-distribution categories (Fig. 8).

Implementing this key requires global distributions of air temperature, topographic variability, and wind speed. Threshold values defining very high (air temperature only), high, and low for these three variables are also necessary. Air temperature distributions and thresholds follow Sturm et al. (1995), who used the Legates and Willmott (1990) 60-yr global climatology of observed monthly mean surface air temperature on a 0.5° latitude–longitude grid. For the current application, these data were resampled to a 2.5-arc-min latitude–longitude grid. Topographic variability was calculated using GTOPO30, a global, 30-arc-s latitude–longitude (approximately 1 km) topographic dataset (Gesch et al. 1999); the standard deviation was calculated for each coincident 2.5-arc-min latitude–longitude grid cell (approximately 5 km), and a threshold of 50 m was used as the boundary between low and high topographic variability. To map the global wind speed variations, the 30-arc-s latitude–longitude, International Geosphere-Biosphere Programme (IGBP) land cover classification was used as a surrogate for wind speed (Sturm et al. 1995). The vegetation data were resampled to a 2.5-arc-min latitude–longitude grid, and the multiple vegetation classes were reduced to two classes: tall (e.g., forests) and short (e.g., grassland, tundra, shrubland, cropland) land cover, which corresponded to low and high wind speeds, respectively. Combining the Fig. 8 decision tree with the thresholds and three datasets yielded nine characteristic snow distribution categories across the globe on a 2.5-arc-min latitude–longitude grid (Fig. 9). Table 1 presents the Northern Hemisphere area covered by each of the nine categories and the percentage of land covered by each category relative to the area covered by categories 2–9. Each category covers substantial land area.

In SSNOWD, a representative coefficient of variation, CV, must be known for each of the categories in Fig. 9. Using observations made as part of published field studies, CVs for each of categories 1–9 were defined. These snow-depth-distribution observations typically come from distributed snow surveys ranging from tens of samples over distances of hundreds of meters, to thousands of samples over distances of tens of kilometers. Ideally, to define CVs for each category, we would have snow-depth-distribution observations on a 10-cm spacing along transects hundreds of kilometers long, but such data do not exist.

A general discussion of each category follows, along with the references used to define the CV values provided in Fig. 9: category 1 relates to an ephemeral snow cover (Sturm et al. 1995) and typically exhibits minimal spatial variability. Category 2 exists in forested, non-

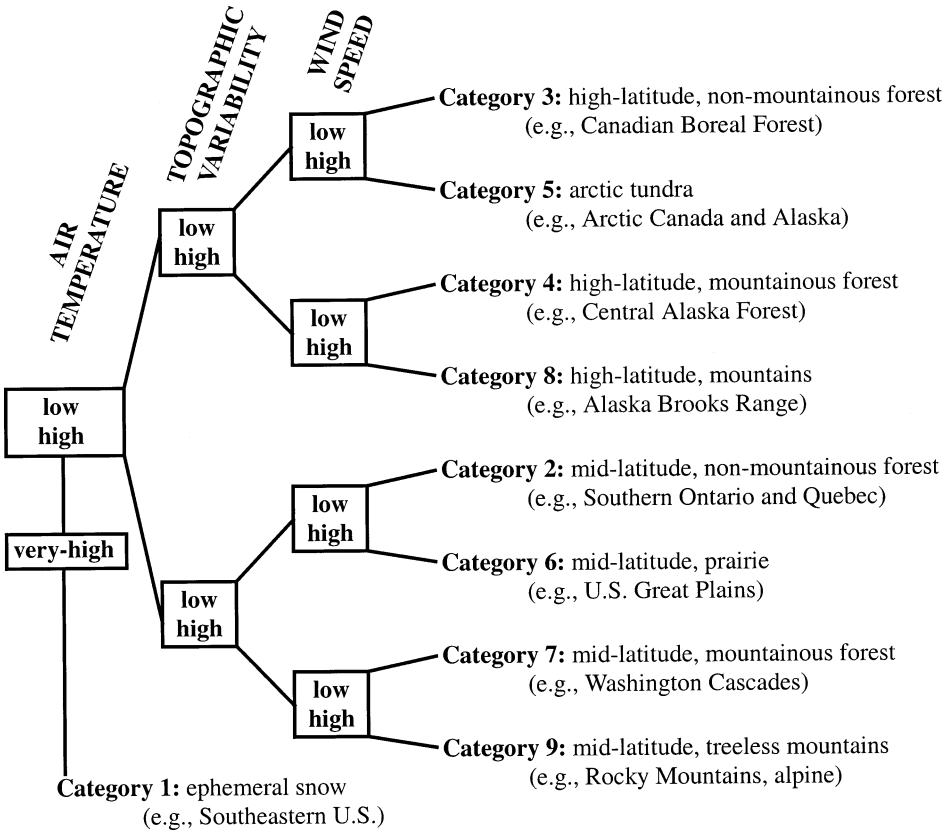

FIG. 8. Dichotomous key used to define the snow-distribution categories. A general description of each category is included, along with an example geographic region where that category can typically be found.

mountainous regions such as the northeastern United States and southern Ontario and Quebec (Buttle and McDonnell 1987; Shanley and Chalmers 1999; Murray and Buttle 2003). Category 3 dominates boreal forest regions (Kuusisto 1980; Woo and Steer 1986; Sturm 1992; Timoney et al. 1992; Pomeroy and Gray 1995; Hedstrom and Pomeroy 1998; Pomeroy et al. 1998, 2002; Faria et al. 2000). Category 4 is similar to category 3, but the boreal forests are in relatively mountainous terrain (see category 3 references). Category 5 is associated with high-latitude grassland/tundra areas, where vegetation is typically short and air temperatures are low (Liston and Sturm 1998, 2002; Essery et al. 1999a; Sturm et al. 2001a; Sturm and Liston 2004). Category 6 corresponds to prairie regions such as those found in central Canada and the United States (Pomeroy et al. 1993; Pomeroy and Gray 1995). Category 7 is characterized by relatively high temperatures (e.g., high compared to the arctic), moderate to high topographic variability, and low wind speeds due to dense forests. Examples include the forested mountain regions of the Rocky Mountains and Canadian coastal ranges where orographic precipitation (due to the topographic variability) is significant (Liston et al. 1999; Marks et al. 2001; Elder et al. 2003, manuscript submitted to *J. Hydrometeor.*). Category 8 corresponds to areas of low temperature, high topographic variability, and strong winds, like the Brooks Range in arctic Alaska, and Svalbard, Norway (Winther et al. 1998; Bruland et al. 2004; Liston and Sturm 2002; R. L. H. Essery, E. M. Blyth, and R. J. Harding 2003, personal communication). Category 9 is distinguished by relatively high temperatures, moderate to high topographic variability, and high wind speeds. Examples include the short-vegetation, windswept regions of Utah and western Colorado and Wyoming (Elder et al. 1991, 1995, 1998; Greene et al. 1999; Balk and Elder 2000; Prasad et al. 2001; Hiemstra et al. 2002).

4. Regional atmospheric model simulations

SSNOWD was tested using a climate version of the Regional Atmospheric Modeling System (ClimRAMS; Liston and Pielke 2001; Cotton et al. 2003), which has been configured for efficient multiyear integrations. Two model simulations were performed: one using the original ClimRAMS snow-covered fraction and energy-balance formulations (the control), the other using SSNOWD. The original snow-cover formulation follows most large-scale atmospheric models, where the surface albedo is adjusted according to a simple formula (the second curve in Fig. 2), and it performs a single

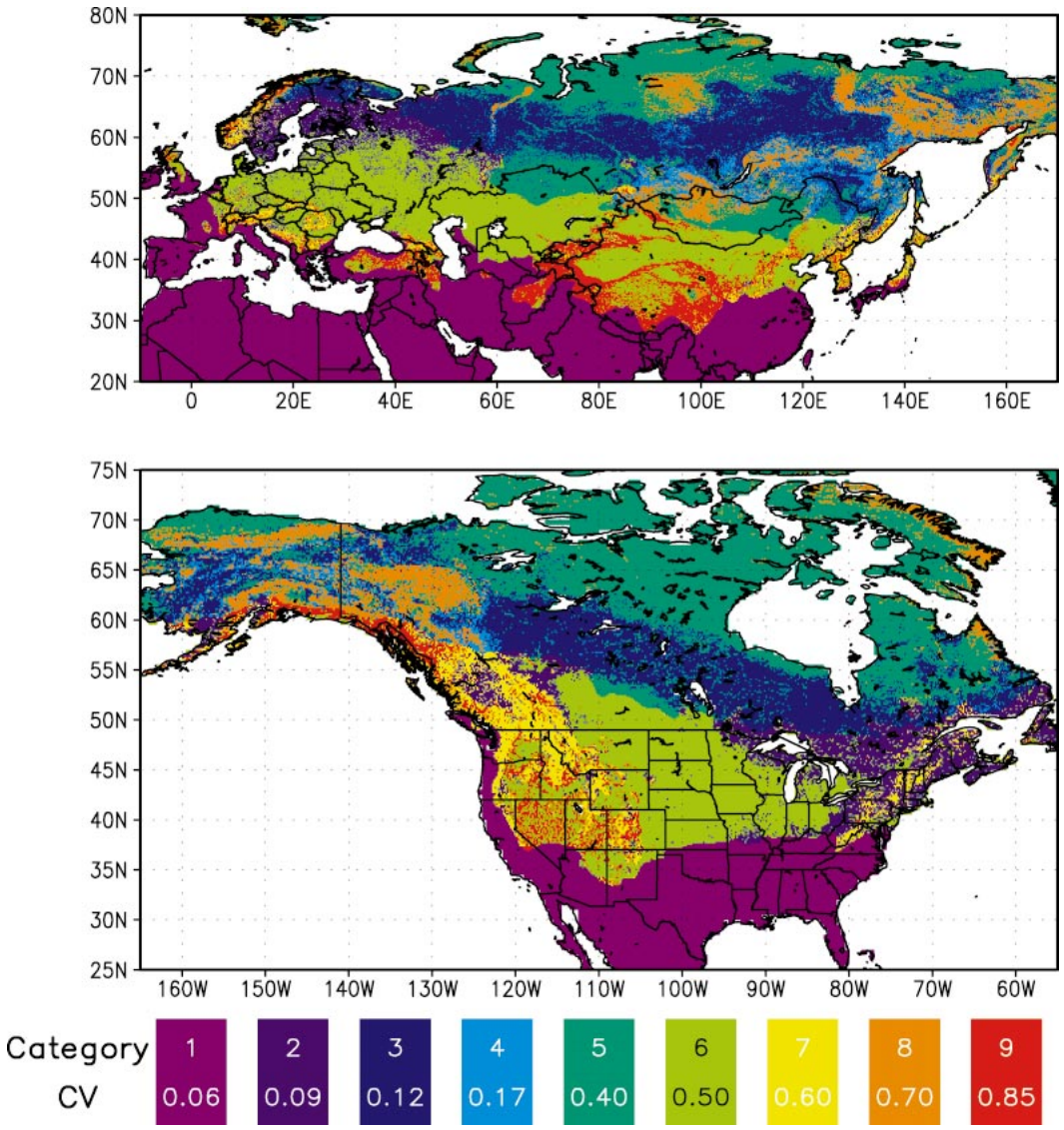

FIG. 9. Global subgrid SWE depth distribution classification determined by the dichotomous key in Fig. 8 (entire world not shown). Also shown are the coefficient-of-variation, CV, values assigned to each category. This 2.5-arc-min lat–lon (approximately 5 km) dataset is available from the National Snow and Ice Data Center, Boulder, CO.

TABLE 1. Area covered by different subgrid snow-distribution categories for the Northern Hemisphere, excluding Greenland. Also shown is the percentage of land covered by each category, relative to the area covered by categories 2–9.

Category	Area (10^6 km^2)	% of categories 2–9
1	47.9	—
2	3.4	6.9
3	8.0	16.2
4	2.2	4.5
5	10.8	21.8
6	14.2	28.7
7	2.3	4.7
8	3.7	7.4
9	4.9	9.8

surface-energy balance. All other aspects of the simulations were identical; for example, SSNOWD subgrid snowmelt moisture was uniformly distributed over the grid cell, and soil temperature calculations did not distinguish between snow-covered and snow-free fractions of each grid cell (i.e., the mean grid-cell snow depth was used in the subsurface thermal and moisture calculations). The simulations are presented as a sensitivity study; no attempt is made to compare the output fields to observed snow distributions. Previous studies assessing the quality of ClimRAMS simulations can be found in Liston et al. (1999) and Liston and Pielke (2001).

For the simulations, ClimRAMS was configured for a domain that included the conterminous United States

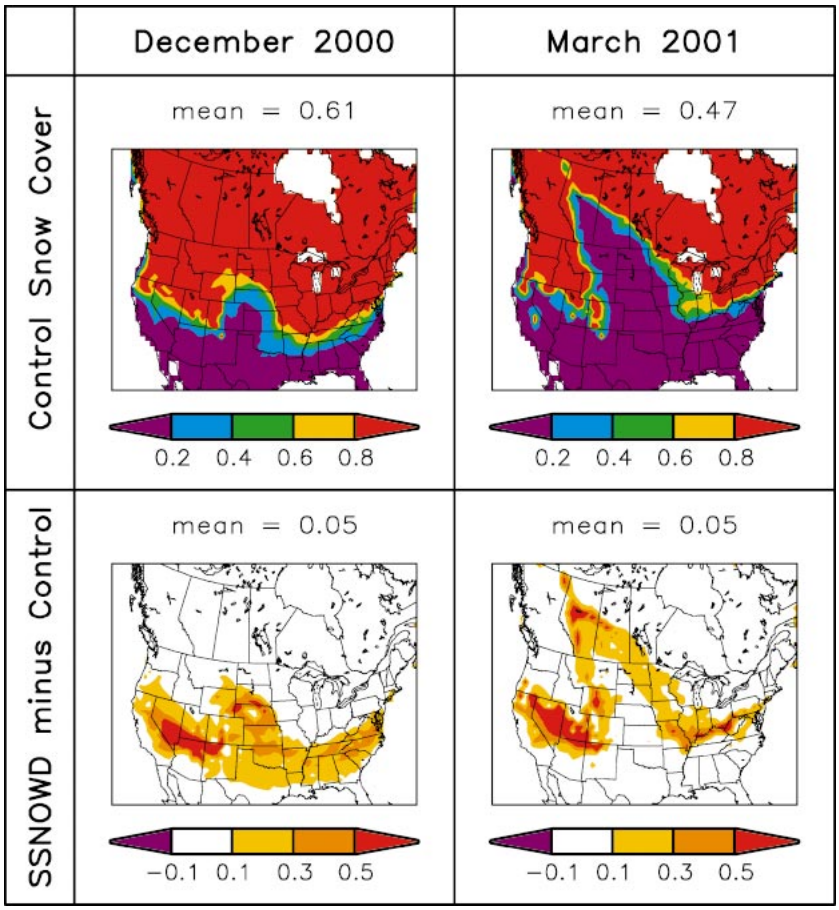

FIG. 10. Monthly average snow-covered area fraction for Dec 2000 and Mar 2001 for two ClimRAMS simulations: one (the control) where the surface albedo was adjusted according to the second curve in Fig. 2 and a single surface-energy balance was performed (this formulation follows most large-scale atmospheric models), and one where SSNOWD was used to represent the subgrid snow-cover distributions. (top) The control simulation, and (bottom) the difference fields (SSNOWD minus control). The means of the distributions are also included.

and most of Canada south of northern Hudson Bay. The simulations spanned a full annual cycle, from 1 September 2000 to 31 August 2001, and used an 80-km horizontal grid increment. This temporal and spatial domain was able to capture the entire seasonal snow-cover evolution over a wide range of climatic regimes and included all nine subgrid snow-distribution categories. The snow-distribution categories (Fig. 9) were matched to the ClimRAMS grid, and each model grid cell was assigned the corresponding CVs. Atmospheric initial and lateral boundary conditions for the simulations (horizontal wind components, relative humidity, air temperature, and geopotential height data) were defined using the National Centers for Environmental Prediction–National Center for Atmospheric Research (NCEP–NCAR) 6-hourly reanalysis products (Kalnay et al. 1996).

Figure 10 highlights how the simulated snow-covered area changed between the control and SSNOWD simulations for December 2000 and March 2001. For both months, the snow-covered area increased under the SSNOWD implementation. Because SSNOWD produces snow-free areas with any simulated snowmelt, we fully expect SSNOWD to develop fractional snow-covered areas during the spring ablation months (as represented by March). In these simulations, even during the winter accumulation season (as represented by December) the snow-covered fraction increased in the southern portions of the domain. This result is expected because this region generally experiences snowmelt shortly following an accumulation event. The spatial distributions are also a function of the CV variations across the domain. For example, the greater snow-covered fractions in the southwestern portions of the United States correspond to the high CV values found there.

Two factors cause SSNOWD to simulate more snow on the ground at the southern edge of the snow-covered domain. First, for nonzero CVs, the assumed subgrid

snow distribution always contains an area of snow that is deeper than the mean. Second, the single surface energy balance, and its associated low albedo values for relatively thin snow covers, melts the snow faster than SSNOWD's two-energy-balance formulation.

Figure 11 presents the correspondence between these snow-covered area variations and surface characteristics and fluxes. For both December and March, 2-m air temperatures were lower, by as much as 5°C, in response to the increased snow-covered area. These temperature differences are consistent with observational and modeling studies of snow-cover influences on air temperature (e.g., Baker et al. 1992; Ellis and Leathers 1999). Runoff (combined surface and base flow) increased along the southern snow-cover boundary and decreased for the areas north of that boundary where snowmelt was not yet fully active. Lower surface temperatures, corresponding to the increased snow cover, lead to increased sensible energy flux (positive toward the surface). The latent energy flux has a similar pattern to the sensible flux, but includes a flux decrease in March over the central United States where the snow-covered fraction differences between the two simulations were minimal.

5. Discussion

Numerous studies have identified the difficulties that many large-scale atmospheric models have in simulating snow evolution and atmospheric processes during the autumn and spring (e.g., Foster et al. 1996; Tao et al. 1996; Frei and Robinson 1998; Lynch et al. 1998). Model improvement efforts have produced advanced snow-albedo formulations and increased vertical resolution of snowpack processes and features. This increase in vertical representation followed a natural model-development progression parallel to the general increase in sophistication of GCM-modeled soil layers. These additional snow layers allow improved representations of snow temperature profiles, snow surface temperatures, and snowpack ''ripening'' during melt. However, from the perspective of the surface energy balance, this only modifies conduction and turbulent flux terms. Because these terms are relatively small over a snow-covered versus a snow-free surface, their impact is not nearly as great as accounting for snow-covered and snow-free grid fractions (Liston 1995).

An additional example of the importance of snow heterogeneity can be found in the case of arctic snowmelt runoff. Without the observed snow-depth heterogeneity, the spring arctic snowmelt discharge hydrograph would be more compressed in time. The snow-depth nonuniformity leads to a snow cover that gradually ablates and moderates the snowmelt runoff. A realistic snow-distribution accounting, where the snow is and where it is not, is a key component of realistically describing snowmelt runoff quantities and timing.

SSNOWD has been developed as a method to address the evolution of the snow-covered area within large-scale atmospheric and hydrologic models. As shown in the ClimRAMS sensitivity simulations, changes in the snow-covered area representation, and the surface-energy-balance computation, can have a significant impact on atmospheric and land surface processes and interactions. While the presentation herein has focused on nonuniform snow distributions over land, the ideas are equally applicable to nonuniform snow distributions on lake ice (e.g., Sturm and Liston 2004) and sea ice (e.g., Sturm et al. 2002a).

In spite of SSNOWD's general applicability to the needs of large-scale models, potential users should be aware of the model's application limits. SSNOWD has been deliberately formulated to be easily available to typical large-scale atmospheric and hydrologic models, and a parameter dataset has been generated to allow global application. These two constraints mean the model, as presented herein, is not entirely general.

For example, the CV values presented in Fig. 9 are not scale independent. They are appropriate for model grid cells of a few kilometers, or greater, on a side. At grid-cell sizes less than this, some of the driving factors that led to the Fig. 9 distributions are no longer appropriate. For example, at grid-cell sizes much less than a few kilometers, the orographic influence on snow-depth variability is no longer valid, leaving only the influence of wind- and vegetation-related snow redistribution. At very small scales, factors we have not considered herein will also influence the CV values. Consider the extreme case of a 1 m by 1 m grid cell; the coefficient of variation will now be dependent upon snow surface-roughness features like dunes, ripples, and sastrugi, and microtopographic features (e.g., rocks and small bumps) of the underlying land surface.

We have also assumed that the CV values are constant with time. This assumption is generally not true in the natural system. Under conditions of melt (even uniform melt) and additional accumulation, the shape of the distribution curve evolves with time. In addition, it is not always appropriate to assume a model grid cell has a uniform melt rate throughout the grid cell. This melt heterogeneity is particularly true in topographically variable terrain and under conditions of local advection. Luce and Tarboton (2001) presented a method to account for this limitation; the main drawback to its use in SSNOWD involves the requirement that CVs evolve with time, adding additional complexity to SSNOWD's formulation and implementation. Pomeroy et al. (2001) also introduced a method to account for subgrid melt distributions, but the data required to implement this globally do not exist.

At longer time scales, significant vegetation changes may occur that would affect snow distribution CVs independent of changes in the physical forcing factors; for example, vegetation changes caused by climate variations (such as different treeline positions or changes in arctic shrub abundance) or land-use change (such as

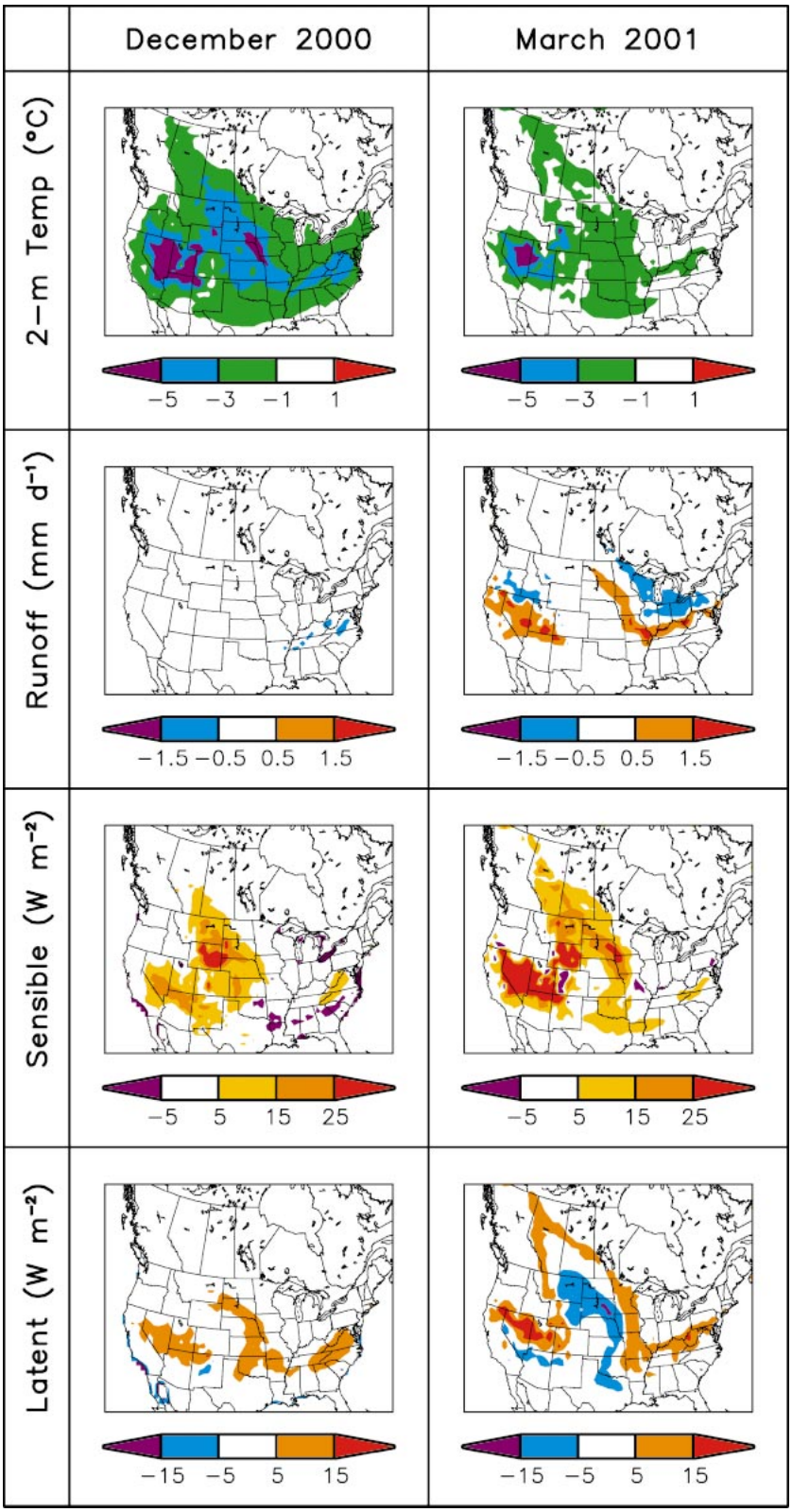

FIG. 11. Monthly average difference plots (SSNOWD minus control), for Dec 2000 and Mar 2001, from the two ClimRAMS simulations described in Fig. 10. Shown are the 2-m air temperature, runoff (positive away from the surface), and sensible and latent heat fluxes (positive toward the surface).

deforestation, agriculture, or urbanization). These differences would require remapping the CVs to reflect the new land surface conditions.

In SSNOWD, it is assumed that there is always some region within each model grid cell that is very thin, such that any snowmelt will yield some fraction of snow-free area. While this is quite appropriate at large spatial scales (e.g., in each grid cell, at least part of some ridge top has nearly been blown free of snow by the wind, or the snow near a tree trunk is very thin), at model grid scales less than a few kilometers an initial snowmelt may not create a snow-free area. This condition can be accommodated by using the three-parameter lognormal distribution (Donald et al. 1995) instead of the two-parameter distribution used by SSNOWD. In this case, the third parameter is an offset that defines the snow-water-equivalent depth that must melt before any snow-free area is created.

6. Conclusions

This study suggests that from both atmospheric and hydrologic perspectives the subgrid snow-depth distribution is an important quantity to include within large-scale climate-related models. Subgrid snow distribution is the critical first-order influence on snow-cover depletion during snowmelt. Liston (1999) showed that three fundamental features are required to describe the evolution of seasonal snow cover from autumn through spring melt. These three features are 1) the within-grid snow-water-equivalent distribution, 2) the grid-cell melt rate, and 3) the within-grid depletion of snow-covered area. During snowmelt, the spatially variable subgrid snow-water-equivalent-depth distribution is largely responsible for the patchy mosaic of snow-covered and snow-free area that develops as the snow melts. Applying the melt rate to a within-grid snow distribution reduces snow-covered area, and the subgrid distribution of snow-free area influences grid-averaged surface fluxes. For the domains of interest in large-scale models, this subgrid snow distribution is most strongly dependent upon spatial variations in snow–canopy interactions, snow redistribution by wind, and orographic precipitation.

These ideas were implemented within a Subgrid SNOW Distribution (SSNOWD) model suitable for application within regional and global weather, climate, and hydrologic models. SSNOWD's formulation benefits from lessons gained in observational studies that have shown that measured snow distributions, in a wide range of environments across the globe, can be reasonably described by a lognormal distribution. With an understanding of the physical processes that create observed snow depths, a global distribution of nine subgrid-snow-variability categories was developed. Coefficient-of-variation values were assigned to each of these categories based on published snow-distribution measurements. Moreover, SSNOWD adopts the physically realistic approach of performing separate surface-energy-balance calculations over snow-covered and snow-free portions of each model grid cell.

A sensitivity test was implemented within ClimRAMS, a regional atmospheric model, over a North American domain. Two model simulations were performed: one using a formulation similar to that currently used in most GCMs and one using SSNOWD. Implementing SSNOWD within a large-scale atmospheric or hydrologic model requires the addition of three two-dimensional model-grid arrays: the first two are accounting arrays that accumulate surface solid (snow) precipitation and snowmelt values, and the third holds CV values for each surface grid cell. Using that information, SSNOWD evolves the fractional snow-covered area in each surface grid cell, at each model time step. This snow-covered fraction is used to partition the surface energy fluxes over the snow-covered and snow-free portions of each grid cell. The annual simulations (September 2000–August 2001) indicated that including realistic snow distributions has a sizable impact on snow-cover evolution and associated surface features as well as energy and moisture fluxes. This influence is particularly critical under snowmelt conditions.

The generation of a methodology addressing subgrid-scale snow-cover variability within the context of large-scale atmospheric and hydrologic models results in key improvements of model-simulated land surface energy and moisture fluxes during the fall, winter, and spring. As such, this research contributes to the next generation of large-scale earth system models that are striving to include improved model realism with respect to subgrid-scale processes. In addition, SSNOWD is applicable to any region of the world where snow is an important feature of the landscape. In these areas, the seasonal cycle of snow cover directly and indirectly influences important aspects of weather, climate, and land surface hydrology.

Acknowledgments. The author would like to thank Yongjiu Dai, Kelly Elder, Richard L. H. Essery, Christopher A. Hiemstra, Joseph P. McFadden, Roger A. Pielke Sr., John W. Pomeroy, John E. Strack, and Kumiko Takata for their insightful reviews of this paper. This work was supported by NOAA Contracts NA67RJ0152 and NA17RJ1228, NASA Grants NAG5-4760 and NAG5-7560, and NSF Grant OPP-0229973-001.

REFERENCES

Ang, A. H. S., and W. H. Tang, 1975: *Probability Concepts in Engineering Planning and Design.* Vol. 1, *Basic Principles*, John Wiley, 409 pp.

Baker, D. G., D. L. Ruschy, R. H. Skaggs, and D. B. Wall, 1992: Air temperature and radiation depressions associated with a snow cover. *J. Appl. Meteor.*, **31,** 247–254.

Balk, B., and K. Elder, 2000: Combining binary decision tree and geostatistical methods to estimate snow distribution in a mountain watershed. *Water Resour. Res.*, **36,** 13–26.

Bamzai, A. S., and J. Shukla, 1999: Relation between Eurasian snow cover, snow depth, and the Indian summer monsoon: An observational study. *J. Climate,* **12,** 3117–3132.

Barros, A. P., and D. P. Lettenmaier, 1994: Dynamic modeling of orographically induced precipitation. *Rev. Geophys.,* **32,** 265–284.

Bonan, G. B., 1996: A land surface model (LSM version 1.0) for ecological, hydrological, and atmospheric studies: Technical Description and User's Guide. NCAR Tech. Note NCAR/TN-417+STR, Boulder, CO, 150 pp.

Bruland, O., G. E. Liston, J. Vonk, and A. Killingtveit, 2004: Modelling the snow distribution at two High-Arctic sites at Svalbard, Norway, and at an Alpine site in Central Norway. *Nord. Hydrol.,* in press.

Buttle, J. M., and J. J. McDonnell, 1987: Modelling the areal depletion of snowcover in a forested catchment. *J. Hydrol.,* **90,** 43–60.

Cotton, W. R., and Coauthors, 2003: RAMS 2001: Current status and future directions. *Meteor. Atmos. Phys.,* **82,** doi:10.1007/s00703-001-0584-9.

Dai, Y., and Coauthors, 2003: The Common Land Model. *Bull. Amer. Meteor. Soc.,* **84,** 1013–1023.

Dewey, K. F., 1977: Daily maximum and minimum temperature forecasts and the influence of snow cover. *Mon. Wea. Rev.,* **105,** 1594–1597.

Dickinson, R. E., A. Henderson-Sellers, and P. J. Kennedy, 1993: Biosphere Atmosphere Transfer Scheme (BATS) Version 1e as coupled to the NCAR Community Climate Model. NCAR Tech. Note NCAR/TN-387+STR, 72 pp.

Donald, J. R., E. D. Soulis, and N. Kouwen, 1995: A land cover-based snow cover representation for distributed hydrologic models. *Water Resour. Res.,* **31,** 995–1009.

Douville, H., J.-F. Royer, and J.-F. Mahfouf, 1995: A new snow parameterization for the Météo-France climate model. Part I: Validation in stand-alone experiments. *Climate Dyn.,* **12,** 21–35.

Edelmann, W., D. Majewski, E. Heise, P. Prohl, G. Doms, B. Ritter, M. Gertz, and T. Hanisch, 1995: Dokumentation des EM/DM-Systems. Deutscher Wetterdienst, 550 pp. [Available from Deutscher Wetterdienst, Zentralamt, D-63004 Offenbach am Main, Germany.]

Elder, K., J. Dozier, and J. Michaelsen, 1991: Snow accumulation and distribution in an alpine watershed. *Water Resour. Res.,* **27,** 1541–1552.

——, J. Michaelsen, and J. Dozier, 1995: Small basin modeling of snow water equivalence using binary regression tree methods. *Biogeochemistry of Seasonally Snow-Covered Catchments,* IAHS Publ. 228, K. Tonnessen, M. Williams, and M. Tranter, Eds., IAHS, 129–139.

——, W. Rosenthal, and R. E. Davis, 1998: Estimating the spatial distribution of snow water equivalence in a montagne watershed. *Hydrol. Processes,* **12,** 1973–1808.

Ellis, A. W., and D. J. Leathers, 1999: Analysis of cold airmass temperature modification across the U.S. Great Plains as a consequence of snow depth and albedo. *J. Appl. Meteor.,* **38,** 696–711.

Essery, R. L. H., 1997: Modelling fluxes of momentum, sensible heat and latent heat over heterogeneous snow cover. *Quart. J. Roy. Meteor. Soc.,* **123,** 1867–1883.

——, L. Li, and J. Pomeroy, 1999a: A distributed model of blowing snow over complex terrain. *Hydrol. Processes,* **13,** 2423–2438.

——, E. Martin, H. Douville, A. Fernandez, and E. Brun, 1999b: A comparison of four snow models using observations from an alpine site. *Climate Dyn.,* **15,** 583–593.

Faria, D. A., J. W. Pomeroy, and R. L. H. Essery, 2000: Effect of covariance between ablation and snow water equivalent on depletion of snow-covered area in a forest. *Hydrol. Processes,* **14,** 2683–2695.

Foster, J., and Coauthors, 1996: Snow cover and snow mass intercomparisons of general circulation models and remotely sensed datasets. *J. Climate,* **9,** 409–426.

Frei, A., and D. A. Robinson, 1998: Evaluation of snow extent and its variability in the Atmospheric Model Intercomparison Project. *J. Geophys. Res.,* **103** (D8), 8859–8871.

Gesch, D. B., K. L. Verdin, and S. K. Greenlee, 1999: New land surface digital elevation model covers the Earth. *Eos, Trans. Amer. Geophys. Union,* **80,** 69–70.

Greene, E. M., G. E. Liston, and R. A. Pielke Sr., 1999: Simulation of above treeline snowdrift formation using a numerical snow-transport model. *Cold Reg. Sci. Technol.,* **30,** 135–144.

Hartman, M. D., J. S. Baron, R. B. Lammers, D. W. Cline, L. E. Band, G. E. Liston, and C. Tague, 1999: Simulations of snow distribution and hydrology in a mountain basin. *Water Resour. Res.,* **35,** 1587–1603.

Hedstrom, N., and J. W. Pomeroy, 1998: Intercepted snow in the boreal forest: Measurement and modelling. *Hydrol. Processes,* **12,** 1611–1625.

Hiemstra, C. A., G. E. Liston, and W. A. Reiners, 2002: Snow redistribution by wind and interactions with vegetation at upper treeline in the Medicine Bow Mountains, Wyoming, USA. *Arct. Antarct. Alp. Res.,* **34,** 262–273.

Jeffries, M. O., T. J. Zhang, K. Frey, and N. Kozlenko, 1999: Estimating late-winter heat flow to the atmosphere from the lake-dominated Alaskan North Slope. *J. Glaciol.,* **45,** 315–324.

Jin, J., X. Gao, Z.-L. Yang, R. C. Bales, S. Sorooshian, R. E. Dickinson, S. F. Sun, and G. X. Wu, 1999: Comparative analyses of physically based snowmelt models for climate simulations. *J. Climate,* **12,** 2643–2657.

Kalnay, E., and Coauthors, 1996: The NCEP/NCAR 40-Year Reanalysis Project. *Bull. Amer. Meteor. Soc.,* **77,** 437–471.

Karl, T. R., P. Y. Groisman, R. W. Knight, and R. R. Heim, 1993: Recent variations of snow cover and snowfall in North America and their relation to precipitation and temperature variations. *J. Climate,* **6,** 1327–1344.

Kirnbauer, R., and G. Blöschl, 1994: How similar are snow cover patterns from year to year? *Dtsch. Gewaesser. Mitteil.,* **37,** 113–121.

Kuusisto, E., 1980: On the values and variability of degree-day melting factor in Finland. *Nord. Hydrol.,* **11,** 235–242.

Legates, D. R., and C. J. Willmott, 1990: Mean seasonal and spatial variability in gauge-corrected, global precipitation. *Int. J. Climatol.,* **10,** 111–127.

Leung, R. L., and S. J. Ghan, 1995: A subgrid parameterization of orographic precipitation. *Theor. Appl. Climatol.,* **52,** 95–118.

Liston, G. E., 1995: Local advection of momentum, heat, and moisture during the melt of patchy snow covers. *J. Appl. Meteor.,* **34,** 1705–1715.

——, 1999: Interrelationships among snow distribution, snowmelt, and snow cover depletion: Implications for atmospheric, hydrologic, and ecologic modeling. *J. Appl. Meteor.,* **38,** 1474–1487.

——, and M. Sturm, 1998: A snow-transport model for complex terrain. *J. Glaciol.,* **44,** 498–516.

——, and R. A. Pielke Sr., 2001: A climate version of the regional atmospheric modeling system. *Theor. Appl. Climatol.,* **68,** 155–173.

——, and M. Sturm, 2002: Winter precipitation patterns in arctic Alaska determined from a blowing-snow model and snow-depth observations. *J. Hydrometeor.,* **3,** 646–659.

——, R. A. Pielke Sr., and E. M. Greene, 1999: Improving first-order snow-related deficiencies in a regional climate model. *J. Geophys. Res.,* **104** (D16), 19 559–19 567.

——, J. P. McFadden, M. Sturm, and R. A. Pielke Sr., 2002: Modeled changes in arctic tundra snow, energy, and moisture fluxes due to increased shrubs. *Global Change Biol.,* **8,** 17–32.

Loth, B., and H.-F. Graf, 1998a: Modeling the snow cover in climate studies. 1. Long-term integrations under different climatic conditions using a multilayered snow-cover model. *J. Geophys. Res.,* **103** (D10), 11 313–11 327.

——, and ——,1998b: Modeling the snow cover in climate studies. 2. The sensitivity to internal snow parameters and interface processes. *J. Geophys. Res.,* **103** (D10), 11 329–11 340.

Luce, C. H., and D. G. Tarboton, 2001: Modeling snowmelt over an

area: Modeling subgrid scale heterogeneity in distributed model elements. *Proc. MODSIM 2001, Int. Congress on Modelling and Simulation,* Canberra, Australia, Australian National University, 341–346.

Lynch, A. H., D. L. McGinnis, and D. A. Bailey, 1998: Snow-albedo feedback and the spring transition in a regional climate system model: Influence of land surface model. *J. Geophys. Res.,* **103** (D22), 29 037–29 049.

Lynch-Stieglitz, M., 1994: The development and validation of a simple snow model for the GISS GCM. *J. Climate,* **7,** 1842–1855.

Marks, D., K. R. Cooley, D. C. Robertson, and A. Winstral, 2001: Long-term snow database, Reynolds Creek Experimental Watershed, Idaho, USA. *Water Resour. Res.,* **37,** 2835–2838.

Marshall, S., and R. J. Oglesby, 1994: An improved snow hydrology for GCMs. Part 1: Snow cover fraction, albedo, grain size, and age. *Climate Dyn.,* **10,** 21–37.

——, J. O. Roads, and G. Glatzmaier, 1994: Snow hydrology in a general circulation model. *J. Climate,* **7,** 1251–1269.

McKay, G. A., and D. M. Gray, 1981: The distribution of snowcover. *Handbook of Snow: Principles, Processes, Management, and Use,* D. M. Gray and D. H. Male, Eds., Pergamon Press, 153–190.

Moore, R. J., V. A. Bell, R. M. Austin, and R. J. Harding, 1999: Methods for snowmelt forecasting in upland Britain. *Hydrol. Earth Syst. Sci.,* **3,** 233–246.

Murray, C. D., and J. M. Buttle, 2003: Impacts of clearcut harvesting on snow accumulation and melt in a northern hardwood forest. *J. Hydrol.,* **271,** 197–212.

Namias, J., 1985: Some empirical evidence for the influence of snow cover on temperature and precipitation. *Mon. Wea. Rev.,* **113,** 1542–1553.

Olyphant, G. A., 1986: Longwave radiation in mountainous areas and its influence on the energy balance of alpine snowfields. *Water Resour. Res.,* **22,** 62–66.

——, and S. A. Isard, 1988: The role of advection in the energy balance of late-lying snowfields: Niwot Ridge, Front Range, Colorado. *Water Resour. Res.,* **24,** 1962–1968.

Pitman, A. J., 2003: The evolution of, and revolution in, land surface schemes designed for climate models. *Int. J. Climatol.,* **23,** 479–510.

Pomeroy, J. W., and D. M. Gray, 1995: Snowcover accumulation, relocation and management. National Hydrology Research Institute Science Rep. 7, NHRI, Environment Canada, Saskatoon, Canada, 144 pp.

——, and R. L. H. Essery, 1999: Turbulent fluxes during blowing snow: Field test of model sublimation predictions. *Hydrol. Processes,* **13,** 2963–2975.

——, D. M. Gray, and P. G. Landine, 1993: The Prairie Blowing Snow Model: Characteristics, validation, operation. *J. Hydrol.,* **144,** 165–192.

——, ——, K. R. Shook, B. Toth, R. L. H. Essery, A. Pietroniro, and N. Hedstrom, 1998: An evaluation of snow accumulation and ablation processes for land surface modeling. *Hydrol. Processes,* **12,** 2339–2367.

——, S. Hanson, and D. Faria, 2001: Small-scale variation in snowmelt energy in a boreal forest: An additional factor controlling depletion of snow cover? *Proc. 58th Eastern Snow Conf.,* Ottawa, Ontario, Canada, Canadian Snow Committee, 85–94.

——, D. M. Gray, N. R. Hedstrom, and J. R. Janowicz, 2002: Prediction of seasonal snow accumulation in cold climate forests. *Hydrol. Processes,* **16,** 3543–3558.

——, B. Toth, R. J. Granger, N. R. Hedstrom, and R. L. H. Essery, 2003: Variation in surface energetics during snowmelt in a subarctic mountain catchment. *J. Hydrometeor.,* **4,** 702–719.

Prasad, R., D. G. Tarboton, G. E. Liston, C. H. Luce, and M. S. Seyfried, 2001: Testing a blowing snow model against distributed snow measurements at Upper Sheep Creek, Idaho, USA. *Water Resour. Res.,* **37,** 1341–1357.

Roesch, A., H. Gilgen, M. Wild, and A. Ohmura, 1999: Assessment of GCM simulated snow albedo using direct observations. *Climate Dyn.,* **15,** 405–418.

——, ——, ——, and ——, 2001: A new snow cover fraction parameterization for the ECHAM4 GCM. *Climate Dyn.,* **17,** 933–945.

Sellers, P. J., and Coauthors, 1996: A revised land surface parameterization (SiB2) for atmospheric GCMs. Part I: Model formulation. *J. Climate,* **9,** 676–705.

Shanley, J. B., and A. Chalmers, 1999: The effect of frozen soil on snowmelt runoff at Sleepers River, Vermont. *Hydrol. Processes,* **13,** 1843–1857.

Shook, K., 1995: Simulation of the ablation of prairie snowcovers. Ph.D. dissertation, University of Saskatchewan, Saskatoon, Canada, 189 pp.

Slater, A. G., A. J. Pitman, and C. E. Desborough, 1998: The validation of a snow parameterization designed for use in general circulation models. *Int. J. Climatol.,* **18,** 595–617.

——, and Coauthors, 2001: The representation of snow in land surface schemes: Results from PILPS 2(d). *J. Hydrometeor.,* **2,** 7–25.

Sturm, M., 1992: Snow distribution and heat flow in the taiga. *Arct. Alp. Res.,* **24,** 145–152.

——, and G. E. Liston, 2004: The snow cover on lakes of the Arctic Coastal Plain of Alaska, USA. *J. Glaciol.,* in press.

——, J. Holmgren, and G. E. Liston, 1995: A seasonal snow cover classification system for local to global applications. *J. Climate,* **8,** 1261–1283.

——, G. E. Liston, C. S. Benson, and J. Holmgren, 2001a: Characteristics and growth of a snowdrift in arctic Alaska. *Arct. Antarct. Alp. Res.,* **33,** 319–329.

——, J. P. McFadden, G. E. Liston, F. S. Chapin III, C. H. Racine, and J. Holmgren, 2001b: Snow–shrub interactions in arctic tundra: A hypothesis with climatic implications. *J. Climate,* **14,** 336–344.

——, J. Holmgren, and D. K. Perovich, 2002a: Winter snow cover on the sea ice of the Arctic Ocean at the Surface Heat Budget of the Arctic Ocean (SHEBA): Temporal evolution and spatial variability. *J. Geophys. Res.,* **107,** 8047, doi:10.1029/2000JC000400.

——, D. K. Perovich, and J. Holmgren, 2002b: Thermal conductivity and heat transfer through the snow on the ice of the Beaufort Sea. *J. Geophys. Res.,* **107,** 8043, doi:10.1029/2000JC000409.

Sun, S., J. Jin, and Y. Xue, 1999: A simple snow-atmosphere-soil transfer model. *J. Geophys. Res.,* **104** (D16), 19 587–19 597.

Takata, K., S. Emori, and T. Watanabe, 2003: Development of the minimal advanced treatments of surface interaction and runoff. *Global Planet. Change,* **38,** 209–222.

Tao, X., J. E. Walsh, and W. L. Chapman, 1996: An assessment of global climate model simulations of Arctic air temperatures. *J. Climate,* **9,** 1060–1076.

Taras, B., M. Sturm, and G. E. Liston, 2002: Snow–ground interface temperatures in the Kuparuk River Basin, arctic Alaska: Measurements and model. *J. Hydrometeor.,* **3,** 377–394.

Timoney, K., G. P. Kershaw, and D. Olesen, 1992: Late winter snow-landscape relationships in the subarctic near Hoarfrost River, Great Slave Lake, Northwest Territories, Canada. *Water Resour. Res.,* **28,** 1991–1998.

Verseghy, D. L., 1991: CLASS—A Canadian land surface scheme for GCMs. I: Soil model. *Int. J. Climatol.,* **11,** 111–133.

Wagner, A. J., 1973: The influence of average snow depth on monthly mean temperature anomaly. *Mon. Wea. Rev.,* **101,** 624–626.

Walland, D. J., and I. Simmonds, 1996: Sub-grid-scale topography and the simulation of Northern Hemisphere snow cover. *Int. J. Climatol.,* **16,** 961–982.

Walsh, J. E., W. H. Jasperson, and B. Ross, 1985: Influences of snow cover and soil moisture on monthly air temperature. *Mon. Wea. Rev.,* **113,** 756–768.

Winther, J.-G., O. Bruland, K. Sand, A. Killingtveit, and D. Marechal, 1998: Snow accumulation distribution on Spitsbergen, Svalbard, in 1997. *Polar Res.,* **17,** 155–164.

Woo, M.-K., and P. Steer, 1968: Monte Carlo simulation of snow depth in a forest. *Water Resour. Res.,* **22,** 864–868.

Yang, Z.-L., R. E. Dickinson, A. Robock, and K. Y. Vinnikov, 1997: Validation of the snow submodel of the biosphere–atmosphere transfer scheme with Russian snow cover and meteorological observational data. *J. Climate*, **10,** 353–373.

Zeng, X., M. Shaikh, Y. Dai, R. E. Dickinson, and R. Myneni, 2002: Coupling of the Common Land Model to the NCAR Community Climate Model. *J. Climate*, **14,** 1832–1854.

Zhang, T., T. E. Osterkamp, and K. Stamnes, 1996: Influence of the depth hoar layer of the seasonal snow cover on the ground thermal regime. *Water Resour. Res.*, **32,** 2075–2086.